Supporting Information: Cell Membrane Poration and Resealing Dynamics in Localized Nanochannel Electroporation

Junjie Pan [1], Chi-ling Chiang [1], Xinyu Wang [1], Paul Bertani [2], Yifan Ma [3], Junao Cheng [2], Vishank Talesara [2], Ly James Lee [1, *] and Wu Lu [2, *]

[1] Department of Chemical and Biomolecular Engineering, The Ohio State University, Columbus, Ohio 43210, USA

[2] Department of Electrical and Computer Engineering, The Ohio State University, Columbus, Ohio 43210, USA

[3] Department of Biomedical Engineering, The Ohio State University, Columbus, Ohio 43210, USA

* Author to whom correspondence should be addressed. Electronic mail: lu.173@osu.edu; lee.31@osu.edu

Table S1. Model geometry and material parameters used in the 2D axisymmetric model.

	Parameter	Value
Geometry	Length of micron well	200 μm
	Radius of micron well	15 μm
	Length of Submicron channel	10 μm
	Radius of Submicron channel	1 μm
	Cell radius	7.5 μm
	Membrane thickness [1]	5 nm
	Gap spacing between cell and channel	10 nm
Material	Extracellular medium conductivity [1]	0.8 S/m
	Cytoplasm conductivity [1]	0.2 S/m
	Cell membrane conductivity [1]	5×10−7 S/m

Table S2. Summary of working conditions for nanochannel electroporation (NEP) using porous substrates in previous works.

Research works	Pore size (μm)	Pore density (/cm^2)	Optimized working voltages	Single pulse duration	Frequency and pulse number
Chang, et al.[2]	D=0.5, L=10	4×10^6	50~140V	10ms ~30ms	10Hz, 1~5 pulses
Fei, et al.[3]	D=0.4	Not mentioned	35V	500ms	1Hz, 5 pulses
Kang, et al. [4]	D=0.6	2×10^7	80V+10V (bilevel)	0.25ms+3ms, (bi-level waves)	200 Hz, 1600 pulses
Chen, et al. [5]	D=0.2	$>10^8$	1~4V	20 ms	1 Hz, 1 pulse
Mukherjee, et al.[6]	D=0.2	5×10^8	10~30V	1~5 ms	1~20 Hz, 100~500 pulses
Cao, et al. [7]	D=0.1, L=20	2×10^7	20~40V	0.2 ms	20 Hz, 400~2400 pulses

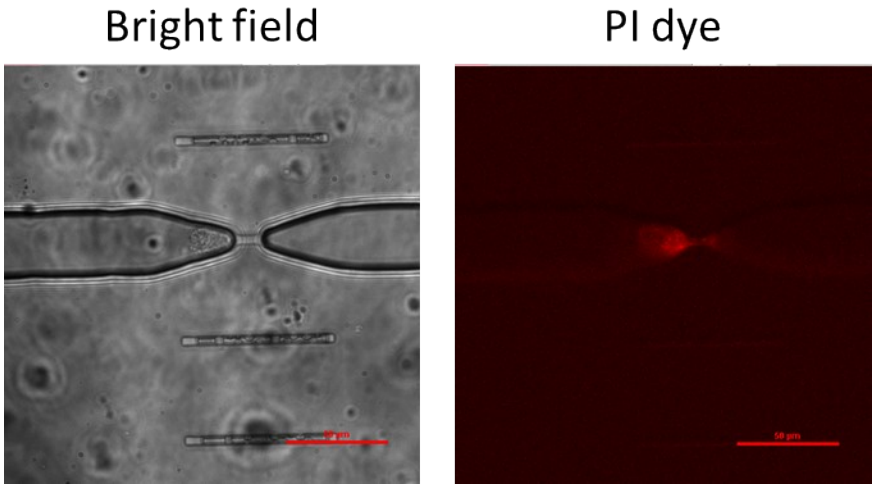

Figure S1. A device used for dynamic current measurement. The chip consisted of only one set of the microchannels to avoid shortcut. A single cell was loaded on one side of the small channel.

1. Electro-osmotic (EO) flow in NEP

In NEP, electrophoresis (EP) is the dominant process to transport the charged molecules into the cell. A brief schematic is shown in Fig. S2 to illustrate the electro-osmotic (EO) and EP effect when delivering negatively charged cargos to the cell. The EP direction is from cathode to anode. However, since the PDMS and glass surface are negatively charged, the EO direction is from anode to cathode, opposite to EP. In NEP, the cell blocks one end of the nanochannel tightly. Therefore, the bulk flow on the cell side was not observed clearly. However, when the cell is not fixed well and not tightly attached to the nanochannel, we observe the bulk flow induced by EO pushing the cell towards the nanochannel (see supplemental video). This verifies the EO direction.

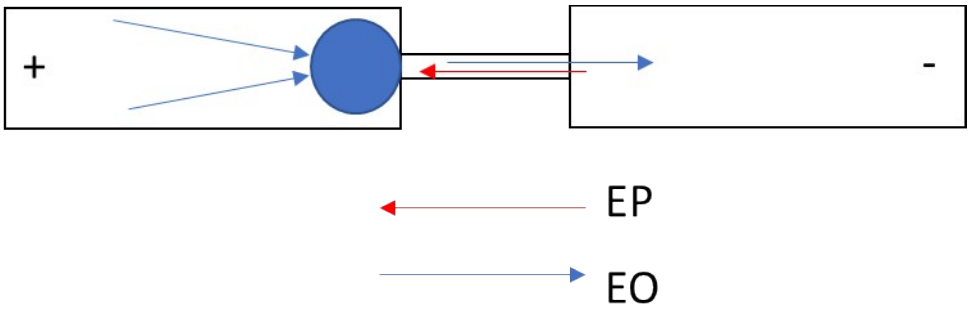

Figure S2. Schematics of electrophoretic (EP) and electro-osmotic (EO) flow in NEP. Electrodes setup for delivering negatively charged cargoes such as FAM-ODN.

NEP setup in Fig. S2 can be widely used for delivery of most biomolecules which are negatively charged such as FAM-ODN. In this case, EO drives the cargoes in the opposite cargo delivery direction, which inhibits mass transport. Even so, EP always plays a dominant role in the cargo transport and thus the overall cargo flux is towards the cell. That's why we see cargo being delivered into the cells in Fig. 2c that FAM ODN is transported to the cell at both 50 and 200V.

2. Joule heating in NEP

We measured dynamic temperature change in NEP device due to Joule heating in our previous work [8]. A simplified schematics is shown in Fig. S2a. Due to the high local electric field strength across nanochannel, nanochannel itself can be treated as a heat source during electric pulse. The temperature inside the nanochannel is the highest in the whole microfluidic device while it drops dramatically at the outlets of the nanochannel. Therefore, only a small portion of the cell that is facing the nanochannel is impacted by the Joule heating.

The temperature gradient in NEP device could induce convective flow as shown in Fig. S2b. The exchange of the fluids between nanochannel and microchannel could facilitate the heat dissipation and reduce the focal heating inside the nanochannel.

In most cases discussed in this study (nanochannel size ~0.8 um, working voltages between 5V to 50V), channel temperature doesn't increase significantly due to Joule heating[2]. This is also one of the reasons why the cell viability high cell viability within this range. Therefore, in terms of cargo transport, the impact of the convective flow could be negligible.

However, under very high working voltages (>150V), the maximum temperature inside the nanochannel could reach close to 100 ^{o}C and sometimes even up to 100 ^{o}C during the electric pulse. In some situations, the high temperature causes water evaporation and induces gas bubble in the nanochannel. Therefore, the impact of the bubble formation as well as convective flow cannot be ignored. Even so, we still observe the higher transfection dose at 200 V as shown in Fig. 2c. This indicates that the complicated flow behavior due to EO, heating induced bubble formation and convective flow at 200V does not change the overall mass transport direction. However, it does impact the electric potential distribution of the whole device and reduce the overall mass flux in comparison with the same electric condition but without such complicated flow behavior.

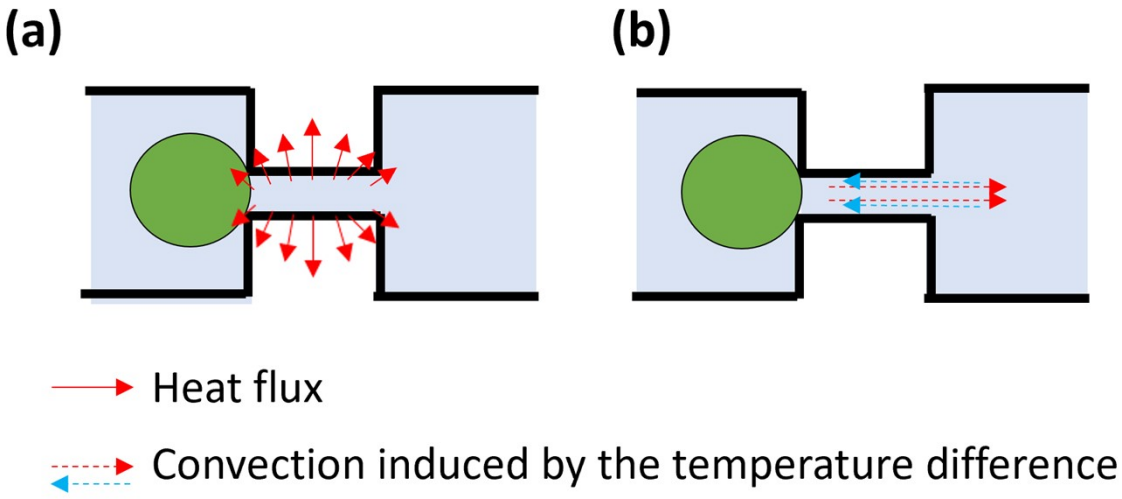

Figure S3. Schematics of joule heating and heat induced convective flow.

3. How EO and Joule heating impact the modeling results?

The 3d model (**Fig. 3**) for t-TMP analysis predicted the electric potential of the whole geometry within nanosecond scale. The bulk flow induced by the EO and Joule heating forms and develops quite a while later after the electroporation starts. Therefore, the bulk flow behavior affected by EO and Joule heating have no impact on the conclusions drawn from **Fig.3**.

The 1d electric circuit model (**Fig.5**) for d-TMP analysis is a time dependent simulation. Therefore, we do need to be very careful about the flow behavior during the electric pulse. In this work, we didn't involve any mass transport simulations but only about electric behaviors. Therefore, if the fluid geometry is kept the same (i.e., no bubble clog in the micro and nanochannel, fluids filled in the entire space of micro and nanochannel), the fluid components (R_{c1}, R_{c2} and R_{c3}) in the circuit model would not be affected significantly. In our d-TMP simulation, we only focused at low voltage situations (5-50V) where no bubble formed, and no fluid geometry changed. This implies that the resistance of the nanochannel and microchannels would all keep the same during the time-

dependent simulation. Therefore, the conclusions from **Fig.5** would not be impacted by the bulk flow (either from EO or heating induced convection).

Also, the impact of the local cellular heating was not significant at low voltage situations (5-50V). The local temperature change (transfection side of the cell) was less than 10 ^{o}C change compared to the room temperature while most portion of the cell still stay at room temperature. Therefore, it would be acceptable that we assumed the cell membrane properties (i.e., cell membrane tension) kept the same during electroporation. Similarly, electric properties of the materials included in this model could also be assumed as constant in the simulated conditions.

However, we did find slight deviation of the simulation results from the experimental results starting from 50V (**Fig.4** vs. **Fig.5**). This was most likely contributed by the hypothesis regarding the cell membrane. At even higher working voltages, the transfection side and non-transfection side membrane could not be treated separately as discussed before. The bulk flow (due to EO and heat induced convection) could induce dynamic change of R_{c1}, R_{c2} and R_{c3} in the circuit model. Also, heating of the cell could also change the R_b and R_t dynamically by reducing the cell membrane tension Γ in Smoluchowski model due to temperature increase (see next few sections for details). That's also why we didn't touch this electric circuit model in 200V cell transfection case.

To conclude, the model used in this study is more suitable for low to medium working voltages, e.g., below 50 V.

4. The lower working voltages needed in NEP and a comparison of the previous works.

The much lower working voltage of NEP compared to BEP can be explained by the simplified electric circuit model as shown in **Fig. 4a**. The model consisted of a couple of components in

series. The fluids inside channels were treated as resistors (R_{c1}, R_{c2}, R_{c3}). The cell membrane was divided into 'transfection side' and 'non-transfection side' membrane which were both treated by a resistor (R_{m1} or R_{m2}) and a capacitor (C_{m1} or C_{m2}) in parallel. The resistance of cytosol was much lower than other components in the model and thus it could be negligible. As a voltage pulse was applied, the cell membrane was first polarized, which only lasted for less than 1 μs before the dielectric breakdown of the cell membrane because of the pore formation [9]. During the polarization or charging process, the voltage drop was mostly localized on the 'transfection side' membrane, because the intact 'transfection side' membrane has a much higher electric resistance compared to all the other components in the electric circuit. Therefore, the transfection side membrane can be easily porated by applying a much lower working voltage than that in BEP.

Also, despite the difference of the porous substrates (pore size, pore density) in the previous works (**Table S2**), their working voltages could be compared directly as a parameter of 'transfection side' membrane poration during the charging process at the very beginning of NEP as discussed above. Their working voltages were mostly between 10 to 80 V [3–7], which is close to the working voltage defined in this study (20-50 V).

5. Equivalent electric circuit model coupled with pore evolution model

The following ODEs describe the conservation of current density of the equivalent electric circuit model shown in **Fig. 4a**:

$$\frac{\partial V_{m1}}{\partial t} = \frac{1}{C_{m1}}\left(\frac{V_{app} - V_{m1} - V_{m2}}{R_c} - \frac{V_{m1}}{R_{m1}}\right) \quad (1)$$

$$\frac{\partial V_{m2}}{\partial t} = \frac{1}{C_{m2}}\left(\frac{V_{app} - V_{m1} - V_{m2}}{R_c} - \frac{V_{m2}}{R_{m2}}\right) \quad (2)$$

Where V_{m1} is the TMP of the transfection side membrane; V_{m2} is the TMP of the non-transfection side membrane; V_{app} is applied working voltage; R_{m1} is resistance of the transfection side membrane; R_{m2} is the resistance of the non-transfection side membrane; C_{m1} is the capacitance of the transfection side membrane; C_{m2} is the capacitance of the non-transfection side membrane; R_c is the total resistance of fluids in micro and nanochannels (R_{c1} + R_{c2} + R_{c3}). All the model parameters were estimated using the method shown in next section.

We followed the methods developed by Mukherjee et al. to correlate the TMP change of the 'transfection side' and 'non-transfection side' membrane (V_{m1} and V_{m2}) to the pore evolution by the Smoluchowski equation [6]:

$$\frac{\partial n(r,t)}{\partial t} = -\nabla \cdot \left(D_p \frac{\partial n}{\partial r} + \frac{D_p}{kT} n \left(\frac{\partial W(\Gamma,V)}{\partial r} \right) \right) \quad (3)$$

where $n(r,t)$ is the pore density (number of pores per unit area) for the pores with a size of r; r is the pore size; $W(\Gamma,V)$ is the energy barrier to form a hydrophilic pore; Γ is the surface tension of the membrane; V is the transmembrane potential and D_p is the pore diffusion coefficient. The pore evolution (eq.3) and the TMP changes (eq.1 and 2) were coupled by the dynamic change of the resistance of the 'transfection side' and 'non-transfection side' membranes.

6. Estimation of model parameters in ODEs from the equivalent electric circuit model

Both conductive fluids inside the channels and cell membranes are treated as ideal components with a uniform cross section and a fixed length. Their resistance and capacitance can be estimated by the following equations:

$$R == \frac{1L}{\sigma A}$$

$$C = \varepsilon \frac{A}{d}$$

where L is the length, A is the cross-section area, σ is the electric conductivity and ε is the electric permittivity. For the cell membranes, their resistance would keep changing dynamically according to the change of TMPs. Therefore, their initial resistances can be estimated first (or the intact membrane resistances). The model parameters in ODEs are summarized in **Table S.2** and **S.3** and the material electric properties are taken from Boukany et al and Liao's study [10,1].

Table S2. Estimation of the fluidic resistance

	Submicron- channel	Micro-channel	Unit
Channel diameter	1.00E-06	3.00E-05	m
Channel length	1.00E-05	3.00E-04	m
Cross section area	7.85E-13	2.83E-09	m^2
Conductivity of fluid	8.00E-01	8.00E-01	S/m
Resistance of the fluids in the channel	1.59E+07	1.33E+05	Ω
Total fluidic resistance (R_c)	1.62E+07		Ω

Table S3. Estimation of resistance and capacitance of the intact cell membrane at t =0 s

Parameters	Symbol	Value	Unit
Cell radius		7.50E-06	m
Membrane thickness	d_m	5.00E-09	m
Area facing channel (transfection side area)	A_{m1}	7.85E-13	m^2
Area not facing channel (non-transfection side area)	A_{m2}	7.06E-10	m^2
Intact membrane conductivity	k_0	5.00E-07	S/m
Membrane permittivity	C_o	4.43E-11	F/m
Non-transfection side membrane resistance	R_{m2}	1.42E+07	Ω
Transfection side membrane resistance	R_{m1}	1.27E+10	Ω
Non-transfection side membrane capacitance	C_{m1}	6.25E-12	F
Transfection side membrane capacitance	C_{m1}	6.95E-15	F

7. Energy barrier function and model parameters in Smoluchowski equation

Smoluchowski equation is used to predict the pore formation on the 'transfection side' and 'non-transfection side' membrane at different TMPs at each time step. The energy function $W(\Gamma,V)$ in Smoluchowski equation is contributed by the external energy needed to overcome energy barrier to form a conductive hydrophilic pore on the cell membrane.

A typical schematic of electropore formation in the phospholipid bilayer is shown in **Fig. S4** where a hydrophobic channel is first generated without any lipid rearrangement and then the lipid heads tilt to form a hydrophilic channel for extracellular medium to pass through. And multiple energy barriers contributed to the total energy barriers to form such a 'hydrophilic' pore in electroporation:

$$W(\Gamma,V) = W_{steric}(r) + W_{edge}(r) + W_{surface}(r,\Gamma) + W_{elec}(r,V)$$

where $W_{steric}(r)$ is the steric repulsion of lipid head groups; $W_{edge}(r)$ is the bending of the lipid around the circumference of a pore; $W_{surface}(r,\Gamma)$ is the interfacial energy and W_{elec} is the electrical energy contribution. The first three terms are quite straightforward regarding the mechanical energy needed to be overcome thermodynamically that only depend on the membrane properties and its interface properties with the surroundings. $W_{elec}(r,V)$ is the electric energy required to form conducting pores. Neu et al. had a detailed derivation of this function in the previous studies [11].

All the model parameters (shown in **Tab. S4**), initial and boundary conditions regarding the Smoluchowski equation are all referred from Mukherjee et al.'s work [6].

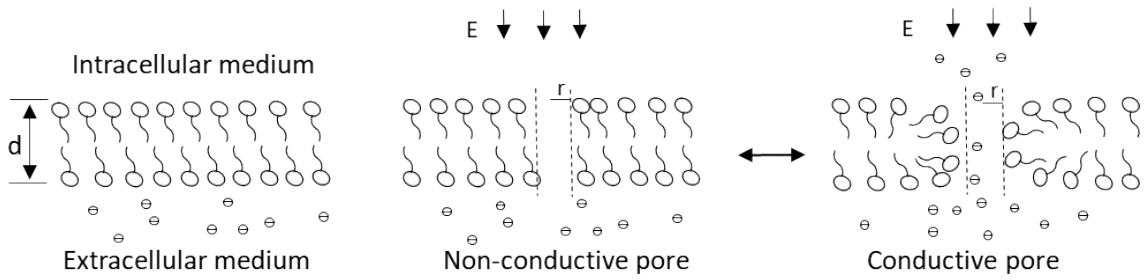

Figure S4. Schematics of the formation of a hydrophilic pore as the cell membrane is subjected to an external electric field.

Table S4 Model parameters used in Smoluchowski equation (for either 'transfection side' or 'non-transfection side' membrane) [6]

Parameters	Symbol	Value	Unit
Pore diffusion coefficient	D_p	2.00E-13	m^2/s
Pore radius	r	Ranging from r_{min} to r_{max} with a step size of 5.00E-11 m	m
Minimum pore size	r_{min}	6.50E-10	m
Maximum pore size	r_{max}	15E-9	m
Energy function	W	$W_{steric}(r) + W_{edge}(r) + W_{surface}(r,\Gamma) + W_{elec}(r,V)$	J/m
Steric repulsion of lipid head groups	$W_{steric}(r)$	$\beta \left(\frac{r_{min}}{r}\right)^4$	J/m
Steric repulsion energy	β	1.40E-19	J/m
Bending of the lipid around the circumference of a pore	$W_{edge}(r)$	$2\pi\gamma$	J/m
Edge energy	γ	2.00E-11	J/m
Interfacial energy	$W_{surface}(r,\Gamma)$	$\Gamma\pi r^2$	J/m
Initial membrane tension	σ	1.00E-04	N/m

Hydrocarbon-water interface tension	σ'	2.00E-02	J/m^2
Total tension of the membrane	Γ	$-2\sigma' + \frac{2\sigma' - \sigma}{(1 - A_f)^2}$	1/m^4
Pore area per unit membrane area	A_f	$\int_{r_{min}}^{r_{max}} n\pi r^2 dr$	
Electrical energy	$W_{elec}(r, V)$	$-\int_{r_{min}}^{r_{max}} \frac{F_{max} V_b^2}{1 + \frac{r_h}{r + r_t}} dr$ (for 'trasnfection side' membrane) $-\int_{r_{min}}^{r_{max}} \frac{F_{max} V_t^2}{1 + \frac{r_h}{r + r_t}} dr$ (for 'non-transfection side' membrane）	J/m
Maximum electric force	F_{max}	6.90E-10	N/V^2
Electric force constant	r_h	9.50E-10	m
Electric force constant	r_t	2.30E-10	m

8. Coupling the Smoluchowski equation with the dynamic TMP change

With Smoluchowski equation, the pore number per unit membrane area (n(r)) and the pore size distribution can be obtained at each time step. The damaged membrane with electro-pores can also be treated as an electric component as shown in **Fig. S5**. Because all the electro-pores can be modeled as resistors in parallel, the total membrane resistance R could be obtained by the following equation:

$$\frac{1}{R} = \frac{1}{R_{intact}} + \sum_{r_{min}}^{r_{max}} \frac{n(r)}{R_r}$$

where R_{intact} is the resistance of the intact membrane without being porated; R_r is the electric resistance of a single pore with a size of r; n is the number of the pores per unit area with a size of r. r_{min} is the minimum pore size; r_{max} is the maximum pore size. Pore size r ranges between r_{min} and r_{max}. **Tab. S5** shows the equations and parameters for predicting the dynamic resistance change of the cell membrane.

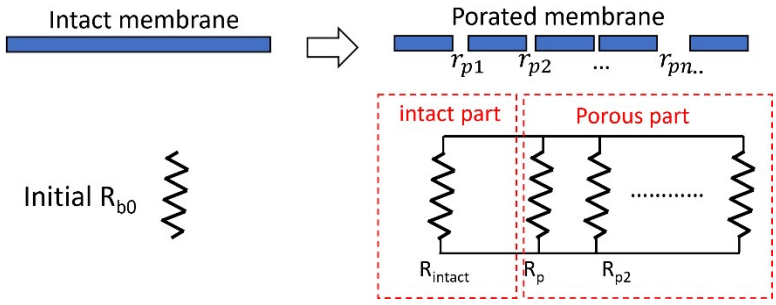

Figure S5. Electro-pore generation and its effect on the total resistance of the cell membrane

Table S5 dynamic change of the electric resistance of the cell membrane and its correlation to the pore evolution [6]

Parameters	Symbol	Expression or value	Unit
Minimum pore size	r_{min}	6.50E-10	m
Maximum pore size	r_{max}	15E-09	m
Porated membrane area per unit area	A_f	$\int_{r_{max}}^{r_{min}} n\pi r^2 dr$	m^2
Pore radius	r	Ranging from r_{min} to r_{max} with a step size of 5.00E-11 m	m
Pore number for each pore size	n(r)	From Smoluchowski equation at each time step	
Transfection side membrane resistance	R_{m1}	$\frac{1}{\frac{1}{R_{intact}} + \sum_{r_{min}}^{r_{max}} \frac{n(r)A}{R_p}}$	Ω
Single pore resistance on 'transfection side' membrane	R_p	$\frac{d_m}{2k_p\pi r^2 K_p H_p} + \frac{1}{2k_p r}$	Ω
Transfection side intact membrane resistance	R_{intact}	$\frac{d_m}{k_0 A_b (1 - A_f)}$	$1/m^2$
Partition factor	K_p	Also, from the study by Mukherjee et al.	
Hinderance factor	H_p	Also, from the study by Mukherjee et al.	

Membrane conductivity	k_0	5.00E-07	S/m
Membrane thickness	d_m	5.00E-09	m
Electro-pore conductivity	k_p	1	S/m

9. Comments on increasing the loading efficiency of single cell in each channel.

In our previous works, multiple cell manipulation approaches have been introduced for loading the cells to the nanochannels for NEP, including optical tweezer[10], magnetic tweezer[12] or dielectrophoretic[13]. They can reach 80~100% single cell loading efficiency. For optical tweezer, each cell is manipulated individually, and the loading efficiency is 100%. However, it is quite time consuming and requires special devices. Also, magnetic tweezer and dielectrophoretic both require cell modification or specific buffer solution. Previous studies involving these few approaches focus on either precise single cell engineering or high throughput cell transfection.

In this study, a few single cells in the microchannel are good enough for a fundamental membrane damage study. Even 30% loading rate can lead to ~60 cells since the total channel number is 200 for each chip. This allows us to have repeats and statistical analysis. Also, empty channels would be fine since all micro-nano-microchannel arrays are in parallel which won't impact each other. Therefore, we use the simplest centrifuge force to load the cells in this work.

10. Reference

(1) Liao, W.-C. Single DNA Dynamics and Cell Electroporation in Micro/Nanofluidics, The Ohio State University, 2012.

(2) Chang, L.; Bertani, P.; Gallego-Perez, D.; Yang, Z.; Chen, F.; Chiang, C.; Malkoc, V.; Kuang, T.; Gao, K.; Lee, L. J.; Lu, W. 3D Nanochannel Electroporation for High-Throughput Cell Transfection with High Uniformity and Dosage Control. *Nanoscale* **2016**, *8* (1), 243–252. https://doi.org/10.1039/C5NR03187G.

(3) Fei, Z.; Wang, S.; Xie, Y.; Henslee, B. E.; Koh, C. G.; Lee, L. J. Gene Transfection of Mammalian Cells Using Membrane Sandwich Electroporation. *Anal. Chem.* **2007**, *79* (15), 5719–5722. https://doi.org/10.1021/ac070482y.

(4) Kang, W.; Giraldo-Vela, J. P.; Nathamgari, S. S. P.; McGuire, T.; McNaughton, R. L.; Kessler, J. A.; Espinosa, H. D. Microfluidic Device for Stem Cell Differentiation and Localized Electroporation of Postmitotic Neurons. *Lab Chip* **2014**, *14* (23), 4486–4495. https://doi.org/10.1039/C4LC00721B.

(5) Chen, Z.; Akenhead, M. A.; Sun, X.; Sapper, H.; Shin, H. Y.; Hinds, Bruce. J. Flow-Through Electroporation of HL-60 White Blood Cell Suspensions Using Nanoporous

Membrane Electrodes. *Adv. Healthcare Mater.* **2016**, *5* (16), 2105–2112. https://doi.org/10.1002/adhm.201600204.
(6) Mukherjee, P.; Nathamgari, S. S. P.; Kessler, J. A.; Espinosa, H. D. Combined Numerical and Experimental Investigation of Localized Electroporation-Based Cell Transfection and Sampling. *ACS Nano* **2018**, *12* (12), 12118–12128. https://doi.org/10.1021/acsnano.8b05473.
(7) Cao, Y.; Ma, E.; Cestellos-Blanco, S.; Zhang, B.; Qiu, R.; Su, Y.; Doudna, J. A.; Yang, P. Nontoxic Nanopore Electroporation for Effective Intracellular Delivery of Biological Macromolecules. *Proc Natl Acad Sci USA* **2019**, *116* (16), 7899–7904. https://doi.org/10.1073/pnas.1818553116.
(8) Pan, J. Measurement and Analysis of Joule Heating in Localized Cellular Micro/Nanochannel Electroporation. In *EIPBN*; 2021.
(9) Krassowska, W.; Filev, P. D. Modeling Electroporation in a Single Cell. *Biophysical Journal* **2007**, *92* (2), 404–417. https://doi.org/10.1529/biophysj.106.094235.
(10) Boukany, P. E.; Morss, A.; Liao, W.; Henslee, B.; Jung, H.; Zhang, X.; Yu, B.; Wang, X.; Wu, Y.; Li, L.; Gao, K.; Hu, X.; Zhao, X.; Hemminger, O.; Lu, W.; Lafyatis, G. P.; Lee, L. J. Nanochannel Electroporation Delivers Precise Amounts of Biomolecules into Living Cells. *Nature Nanotech* **2011**, *6* (11), 747–754. https://doi.org/10.1038/nnano.2011.164.
(11) Neu, J. C.; Smith, K. C.; Krassowska, W. Electrical Energy Required to Form Large Conducting Pores. *Bioelectrochemistry* **2003**, *60* (1–2), 107–114. https://doi.org/10.1016/S1567-5394(03)00051-3.
(12) Chang, L.; Howdyshell, M.; Liao, W.-C.; Chiang, C.-L.; Gallego-Perez, D.; Yang, Z.; Lu, W.; Byrd, J. C.; Muthusamy, N.; Lee, L. J.; Sooryakumar, R. Magnetic Tweezers-Based 3D Microchannel Electroporation for High-Throughput Gene Transfection in Living Cells. *Small* **2015**, *11* (15), 1818–1828. https://doi.org/10.1002/smll.201402564.
(13) Chang, L.; Gallego-Perez, D.; Zhao, X.; Bertani, P.; Yang, Z.; Chiang, C.-L.; Malkoc, V.; Shi, J.; Sen, C. K.; Odonnell, L.; Yu, J.; Lu, W.; Lee, L. J. Dielectrophoresis-Assisted 3D Nanoelectroporation for Non-Viral Cell Transfection in Adoptive Immunotherapy. *Lab Chip* **2015**, *15* (15), 3147–3153. https://doi.org/10.1039/C5LC00553A.